Atomic RABBITT-like experiments framed as diatomic molecules

2016 J. Phys. B: At. Mol. Opt. Phys. 49 185601

(http://iopscience.iop.org/0953-4075/49/18/185601)

IOP Publishing Journal of Physics B: Atomic, Molecular and Optical Physics
J. Phys. B: At. Mol. Opt. Phys. **49** (2016) 185601 (10pp) doi:10.1088/0953-4075/49/18/185601

Atomic RABBITT-like experiments framed as diatomic molecules

D I R Boll[1] **and O A Fojón**[1,2]

[1] Instituto de Física Rosario, CONICET-UNR, Blvd. 27 de Febrero 210 bis, 2000 Rosario, Argentina
[2] Escuela de Ciencias Exactas y Naturales, FCEIA Universidad Nacional de Rosario, Argentina

E-mail: boll@ifir-conicet.gov.ar

Received 6 May 2016, revised 24 June 2016
Accepted for publication 1 July 2016
Published 5 September 2016

Abstract

The single ionization of noble gas atoms by an attosecond pulse train assisted by an infrared laser field is theoretically investigated by means of a non-perturbative model that under certain approximations gives closed-form expressions for the angular distributions of photoelectrons. A very good agreement between our predictions and experiments is observed. Interestingly, our model allow us to interpret these angular distributions as two-center interferences where the separation between centers is governed by the infrared laser field. Finally, we provide a physical interpretation for the analogy of the two-center interferences.

Keywords: atoms, photoionization, attopulses, laser

(Some figures may appear in colour only in the online journal)

1. Introduction

Since the first realization of attosecond pulse trains in 2001 [1, 2], the theoretical effort and the development of tools to scrutinize the electron dynamics in this time scale attracted increasing attention, just because typical orbiting times of valence electrons are hundreds of attoseconds. After that, many works that oriented to the theory and/or experimental field, together with the subsequent diversification of techniques, have built the realm of attophysics in which the coherent control of electron dynamics, in atoms or molecules, emerged as one of the most fascinating perspectives. Moreover, the control of electron localization in dissociating molecular states [3] and the control of orbital parity mix [4] have been proved to be valid tools to steer dynamical properties in reactions.

When atomic or molecular targets are exposed to the simultaneous action of an attosecond pulse train of odd harmonics and a low intensity near infrared laser (NIR) field, the reconstruction of attosecond beating by interference of two-photon transition (RABBITT) scheme is obtained. The photoelectron spectrum contains dressed harmonic lines mainly populated by the absorption of a given harmonic in the attopulse train, and sideband lines associated to the further exchange of one NIR photon. The magnitude of these sidebands oscillates at twice the NIR frequency when the delay between the NIR and the train is modified. This measurement scheme lies at the heart of the attosecond physics allowing, for example, the reconstruction of the time structure of attosecond pulse trains [1] and the time delay determination in photoionization [5]. The intermediate NIR intensity regime, where the exchange of more than one NIR photon is expected, has received much less attention. The presence of many interfering quantum channels requires a treatment beyond the second-order perturbation theory [1, 4].

The theoretical approach to these problems is not simple at all. Solving the time dependent Schrödinger equation (TDSE) for reactions such as the photoionization of multielectron atomic targets assisted by an NIR represents a computational challenge [6] for current computational resources. The use of simplified models leading to predictions in reasonable agreement with *ab initio* calculations and/or experimental results reveals as a valuable option to understand the physical processes involved, as the numerical results do not often have a straightforward interpretation. Nowadays, several models able to describe reactions assisted by a stronger NIR are available. Among them, the soft-photon approximation [7] was successfully applied to study angular distributions in laser-assisted atomic photoionization by photons from free electron laser [8] or high harmonic generation [6, 9] sources. Moreover, the separable Coulomb–Volkov (SCV) model came out as a versatile alternative to

provide in certain situations quite accurate results or at least in qualitative agreement with *ab initio* calculations for atomic or molecular targets [10–12]. Briefly, in the SCV approach there are three time steps in the electronic evolution. In the first one (rapid), absorption of one energetic photon is produced and the ionized electron evolves exclusively in the presence of the Coulomb field of the residual target whereas in the third one (slow), it moves under the exclusive influence of the NIR laser. In the intermediate step, both the Coulomb residual target and the NIR laser fields are acting on the ejected electron.

The sophisticated techniques involved in the measurement of energy-resolved and angle-resolved spectra have evolved in an outstanding way. The long-term stability of the synchronization between the train of attopulses and the assistant laser, necessary for this kind of experiment in cold target recoil ion momentum spectroscopy devices, was reduced to about 60 attoseconds [9, 13], enabling thus the determination of the angular distribution of photoelectrons with a given energy and an almost fixed delay. Experimental studies concerned with these angular distributions, although scarce, showed a critical dependence with the delay [9, 13–17]. The global shape of angle-resolved photoelectron spectra in dressed harmonic lines changes significantly for different delays, in contrast to the sideband lines that, after normalization, are almost insensitive to the delay change [9]. In this context, the angular distributions pose a stringent test to the theoretical predictions.

Here, we present the results of a non-perturbative model that can be considered as an extension of the SCV one. Under certain approximations, this extended model leads to analytical expressions for the angular distribution of photoelectrons in the laser-assisted photoionization reaction. Interestingly, the angle-resolved photoelectron spectra for atomic targets can be interpreted as the ones coming from spatial two-center interferences observed in diatomic molecules.

Atomic units are used throughout unless explicitly stated.

2. Theory

Let us consider the photoionization of atomic targets by a train of attopulses arising from high-order harmonic generation assisted by a monochromatic laser in the near infrared region. As the intensity of each harmonic in the train is low, they may ionize the target only through single photon processes [1] and, thus, the interaction of the active electrons in the atom with the train of attopulses (the first stage of the SCV approach) may be treated in the frame of the time-dependent perturbation theory [6, 18]. On the other hand, the assistant laser field may easily induce multiphoton transitions in the continuum (the third stage of the SCV approach) requiring a non-perturbative treatment. Therefore, the transition matrix amplitude within the dipole approximation in the velocity gauge is given by,

$$M_{\mathrm{SCV}}(\mathbf{p}) = -\mathrm{i}\int_{-\infty}^{\infty} \mathrm{d}t\ \langle \Psi_f(\mathbf{r},t)|\mathbf{A}(t)\cdot\hat{\mathbf{p}}|\Psi_i(\mathbf{r},t)\rangle, \qquad (1)$$

where $\mathbf{p}$ is the photoelectron momentum associated to the momentum operator $\hat{\mathbf{p}}$ and $\Psi_{i,f}(\mathbf{r},t)$ are the wavefunctions in the initial and final channels of the reaction, respectively. The vector potential $\mathbf{A}(t)$ represents the attosecond pulse train (APT) and it can be expressed as a combination of harmonics with Gaussian envelope

$$\mathbf{A}(t) = \mathbf{\Pi}\sum_j A_j \mathrm{e}^{-\mathrm{i}j\omega_0 t}\mathrm{e}^{\mathrm{i}\phi_j}\mathrm{r}^{-t^2/2\tau_T^2}, \qquad (2)$$

where $\mathbf{\Pi}$ is the polarization vector, ω_0 is the fundamental frequency and ϕ_j is the individual phase of each frequency component whose amplitude is given by A_j, respectively. The full width half maximum (FWHM) duration of the train is related to the parameter τ_T through the expression $\tau_{\mathrm{FWHM}} = 2\sqrt{2\ln 2}\,\tau_T$.

The effect of the assistant laser field on the initially bound atomic states has been considered previously [18–20], showing that bound-continuum transitions from atomic states with large ionization and excitation energies are barely affected when the laser field intensity is small or moderate and the photoelectron energy is sufficiently far from the ionization threshold. Therefore, we neglect the polarization and the ionization due to the assistant laser field. Under this approximation, the state of the system in the initial channel of the reaction may be described by the laser-free wavefunction

$$\Psi_i(\mathbf{r},t) \approx \psi_i(\mathbf{r})\mathrm{e}^{\mathrm{i}I_p t}, \qquad (3)$$

where I_p is the ionization potential associated to the initial atomic orbital $\psi_i(\mathbf{r})$.

The final channel of the reaction, where the interaction between the photoelectron and the assistant laser field is treated to all orders, is represented through the ansatz [10, 12]

$$\Psi_f(\mathbf{r},t) \approx \psi_f(\mathbf{r})\exp\left\{-\frac{\mathrm{i}}{2}\int^t [\mathbf{p}+\mathbf{A}_L(t')]^2\mathrm{d}t'\right\}, \qquad (4)$$

where $\psi_f(\mathbf{r})$ is the laser-free continuum wavefunction with asymptotic momentum $\mathbf{p}$. The importance of including the Coulomb interaction between the released photoelectron and the parent ion, particularly for photoelectrons with relatively low kinetic energy, has been revealed in the past [18, 20]. A widespread theoretical approach to account for this interaction, leading to analytic results, is to use the wavefunction

$$\psi_f(\mathbf{r}) = (2\pi)^{-3/2}\mathrm{e}^{\mathrm{i}\mathbf{p}\cdot\mathbf{r}}N_p G(\mathbf{r}), \qquad (5)$$

that represents asymptotically the Coulomb interaction of the residual target with the photoelectron, where, $N_p = \mathrm{e}^{\pi\nu/2}\,\Gamma(1+\mathrm{i}\nu)$, $\nu = Z_f/p$ where Z_f is the net charge of the residual target and $G(\mathbf{r}) = {}_1F_1(-\mathrm{i}\nu;\,1;\,-\mathrm{i}(pr+\mathbf{p}\cdot\mathbf{r}))$ is the confluent hypergeometric function.

For the sake of simplicity, we consider an assistant laser field with polarization collinear to the APT one, with vector potential $\mathbf{A}_L(t)$ given by,

$$\mathbf{A}_L(t) \simeq -\frac{\mathbf{E}_1}{\omega_0}\sin(\omega_0 t - \phi_L) \qquad (6)$$

and, consequently,

$$\mathbf{E}_L(t) = -\frac{\partial \mathbf{A}_L(t)}{\partial t} \simeq \mathbf{E}_1\cos(\omega_0 t - \phi_L) \qquad (7)$$

where E_1 is the amplitude of the corresponding electric field and $\phi_L = \omega_0 t_0$ is an arbitrary phase that allows to modify the delay t_0.

It can be shown that the replacement of equations (2), (3), (4) and (6) into (1), leads to the following expression for the transition matrix amplitude,

$$M_{\mathrm{SCV}}(\mathbf{p}) = -\mathrm{i}\sqrt{2\pi}\,\tau_T M_{ph}(\mathbf{p}) \sum_{m,n=-\infty}^{\infty} \sum_j i^n (-1)^m A_j J_m(M) J_n(N) \mathrm{e}^{-\mathrm{i}(2m+n)\phi_L} \mathrm{e}^{\mathrm{i}\phi_j} e^{-\omega_j^2 \tau_T^2/2}, \tag{8}$$

where we have defined,

$$M = E_1^2/(2\omega_0)^3, \tag{9}$$

$$N = \mathbf{p}\cdot\mathbf{E}_1/\omega_0^2, \tag{10}$$

$$\omega_j = p^2/2 + I_p + (2M + 2m + n - j)\,\omega_0, \tag{11}$$

where $p = |\mathbf{p}|$ is the asymptotic momentum modulus and $M_{ph}(\mathbf{p})$ is the monochromatic transition matrix element describing the single photon ionization from the initial state $\psi_i(\mathbf{r})$ to the final state $\psi_f(\mathbf{r})$.

As far as we are aware, general closed-form expressions for the above summations are not known. However, we will obtain analytical expressions under some simplifying assumptions. Here, our interest is focused on the differential cross sections of dressed harmonic (DH) lines or sideband (SB) lines, satisfying the energy relation $p_q^2/2 + I_p + 2M\omega_0 = q\omega_0$.

If the APT is a combination of odd harmonics, the SB lines result from the interference of energy-degenerate continuum states associated with the absorption of different harmonics from the APT and the exchange of an odd number of NIR photons. In the low NIR intensity limit they are mainly populated by transitions involving the absorption of either two consecutive odd harmonics of the APT plus the absorption and emission of one NIR photon, respectively. Accordingly, they are described by an even integer number q and their transition matrix amplitude is given by (see appendix)

$$M_{\mathrm{SCV}}(\mathbf{p}_q) = \mathrm{i}B_0 M_{ph}(\mathbf{p}_q)\mathrm{e}^{\mathrm{i}M\sin(2\phi_L)}\sin(N\cos\phi_L), \tag{12}$$

where B0 is defined in equation A2.

On the other hand, DH lines represent the interference of energy-degenerate continuum states associated with the absorption of different harmonics from the APT and the exchange of an even number of NIR photons. In the low NIR intensity limit these lines are mainly populated by the transition involving the absorption of a given harmonic in the APT. Accordingly, they are described by an odd integer number q and their transition matrix amplitude is given by (see the appendix)

$$M_{\mathrm{SCV}}(\mathbf{p}_q) = B_0 M_{ph}(\mathbf{p}_q)\mathrm{e}^{\mathrm{i}M\sin(2\phi_L)}\cos(N\cos\phi_L). \tag{13}$$

In every case considered, the constant M appears as a global phase indicating that, independently of the NIR intensity, the oscillatory term that comes from A_L^2 in the Volkov phase can be omitted.

The transition matrix amplitudes in equations (12) and (13) can be used to calculate the differential cross section of SB and DH lines as

$$\frac{\mathrm{d}\sigma}{\mathrm{d}\Omega_e}(\mathbf{p}_q) \propto |M_{ph}(\mathbf{p}_q)|^2 \sin^2(N\cos\phi_L), \tag{14}$$

$$\frac{\mathrm{d}\sigma}{\mathrm{d}\Omega_e}(\mathbf{p}_q) \propto |M_{ph}(\mathbf{p}_q)|^2 \cos^2(N\cos\phi_L), \tag{15}$$

respectively, where $\mathrm{d}\Omega_e = \sin\theta_e \mathrm{d}\theta_e \mathrm{d}\phi_e$ is the differential solid angle element in the photoelectron emission direction as measured from the polarization vector $\mathbf{\Pi}$.

Before we proceed any further, let us check that the above expressions reproduce the expected behavior in the low NIR intensity limit, where $N < 1$. A first-order approximation of the sine function in equation (14) yields a result proportional to $(1 + \cos 2\phi_L)$, that is, an oscillation at twice the NIR frequency, which is the expected result for SB lines. An analogous expansion of the cosine factor in equation (15) indicates, as expected, that DH lines do not oscillate as a function of the delay in the low NIR intensity limit.

Moreover, these results suggest an interesting analogy. Recalling that $N = \mathbf{p}\cdot\mathbf{E}_1/\omega_0^2$, then we define $\mathbf{R}_L = 2\mathbf{E}_1\cos(\phi_L)/\omega_0^2$ and replace it into equations (14) and (15) to obtain the following expressions for the differential cross sections of SB and DH lines,

$$\frac{\mathrm{d}\sigma}{\mathrm{d}\Omega_e}(\mathbf{p}_q) \propto |M_{ph}(\mathbf{p}_q)|^2 \sin^2(\mathbf{p}_q\cdot\mathbf{R}_L/2), \tag{16}$$

$$\frac{\mathrm{d}\sigma}{\mathrm{d}\Omega_e}(\mathbf{p}_q) \propto |M_{ph}(\mathbf{p}_q)|^2 \cos^2(\mathbf{p}_q\cdot\mathbf{R}_L/2), \tag{17}$$

respectively. A physical interpretation of the interference factors in equations (16) and (17) as well as the vector $\mathbf{R}_L$ is given below.

We point out here that the differential cross sections for the ionization of an atom by a sequence of in-phase odd harmonics in the presence of an NIR are analogous to those of the monochromatic ionization of a homonuclear diatomic molecule with internuclear separation $\mathbf{R}_L$, oriented collinearly to the NIR [21–24].

For SB lines it can be seen that equation (16) predicts the existence of a nodal plane for emission perpendicular to $\mathbf{R}_L$ or, equivalently, to the NIR polarization direction, irrespective of the photoelectron momentum modulus, the laser field intensity or the delay. On the contrary, DH lines according to equation (17) exhibit a constructive interference for this situation.

These facts resemble the findings for impact of massive particles on homonuclear diatomic molecules [24] where the classical emission perpendicular to the internuclear vector is forbidden (allowed) for final *ungerade* (*gerade*) states in ionization from the ground (*gerade*) state. In the same way as for massive particles, the interference factors appearing in equation (16) may be related to the interference pattern corresponding to two point sources emitting waves in counter-phase, whereas, the interference predicted by equation (17) may be interpreted as the ones coming from in-phase emitters [24]. The emission at other angles strongly

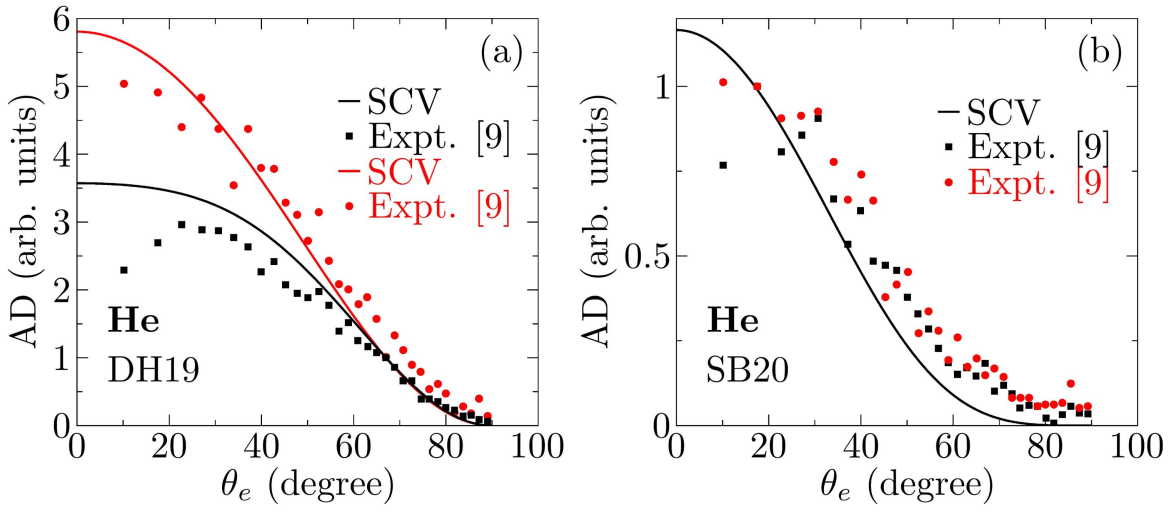

Figure 1. (a) Helium APT-NIR angular distributions for the DH19 line with $\phi_L = 0.14\pi$ (black) and $\phi_L = 0.64\pi$ (red). (b) Same as (a) but for the SB20 line with $\phi_L = 0.14\pi$ (black). The asymptotic photoelectron energy is (a) $p_q^2/2 = 4.76$ eV and (b) $p_q^2/2 = 6.30$ eV.

depends on the relation between the separation $\mathbf{R}_L$ of the sources and the photoelectron wavelength $\lambda_q = 2\pi/p_q$.

To calculate the photoionization differential cross sections (or alternatively, the angular distributions) for atomic targets by using equations (16) and (17), we need to compute the corresponding monochromatic transition amplitudes which are proportional to the square modulus of the transition matrix element $M_{ph}(\mathbf{p}_q)$. Now, provided that the magnetic sublevels of the atomic target are equally populated, the differential cross sections for photoionization by linearly polarized monochromatic radiation has the general form [25],

$$\frac{\mathrm{d}\sigma}{\mathrm{d}\Omega_e}(\mathbf{p}_q) = \frac{\sigma_{\mathrm{tot}}}{4\pi}[1 + \beta P_2(\cos\theta_e)] \propto |M_{ph}(\mathbf{p}_q)|^2, \qquad (18)$$

where σ_{tot} is the total photoionization cross section, β is the asymmetry parameter, $P_2(x) = (3x^2 - 1)/2$ is the second-order Legendre polynomial.

3. Results

In what follows, our analytical results are applied to calculate angular distributions (ADs) in the laser-assisted photoionization of noble gas atoms. The considered attosecond pulse trains are a combination of in-phase odd harmonics of the fundamental frequency $\omega_0 = 0.056855$ a.u. (801.4 nm), and both the APT and the NIR are linearly polarized along the same direction. Our results are compared with recent experimental and theoretical results.

In figure 1, our results for the laser-assisted photoionization of He atoms are compared to the available experimental data [9]. We consider an NIR of intensity $I_L = 0.8 \times 10^{12}$ W cm^{-2}, in agreement with the observed shifts due to the ponderomotive energy [9]. The $\beta = 2$ value used to obtain the ADs is extracted from [25], where a $\cos^2\theta_e$ dependence is predicted for the monochromatic photoionization of an s-type electron. The ADs in figure 1(a) and (b) are normalized for the emission angles 67° and 17°, respectively, preserving thus the normalization of the original experimental data [9].

In figure 1(a), the ADs of the DH19 line evolve notably by changing the delay ϕ_L, particularly for emission in directions close to the polarization axis ($\theta_e = 0°$). In addition, as in these ADs the distance between the sources $\mathbf{R}_L$ is smaller than half the wavelength of the ejected photoelectron, according to equation (17) no total destructive interferences are expected regardless of the emission angle. However, the emission at angles θ_e near 0° reflects the path difference expected for different delays as a change in the interference factor of equation (17). On the contrary, for emission in the direction $\theta_e = 90°$ total constructive interferences are expected but the monochromatic ADs given by equation (18) are proportional to $\cos^2\theta_e$, which gives a zero value for the ADs at $\theta_e = 90°$ due to the dipole selection rules. The discrepancies with the experimental data [9] observed at emission angles $\theta_e < 20°$ are unlikely to result from the approximations in our analytical model. For instance, we performed a non-linear fitting of the data with a partial sum of equation (8) including the most relevant contributions and considering six free parameters (amplitude and phase of each contribution). We found that the description of the experimental ADs at $\theta_e < 20°$ is not enhanced by this procedure.

On the other hand, the shape of the AD in the SB20 (figure 1(b)) does not show a significant dependence with the delay after normalization. The results for the SBs may be understood taking into account that under the present conditions they are populated mainly by two-photon transitions. So, an expansion of the sine factor in equation (14) into Bessel functions and retaining only the first term leads to,

$$\frac{\mathrm{d}\sigma}{\mathrm{d}\Omega_e}(\mathbf{p}_q) \propto |J_1(N)|^2 |M_{ph}(\mathbf{p}_q)|^2 \cos^2\phi_L \qquad (19)$$

where the delay dependence turns out to be a scaling factor, that, considered as a function of the delay oscillates at twice the NIR frequency. This result, valid only when the SBs are populated mainly by two-photon transitions, is similar to the

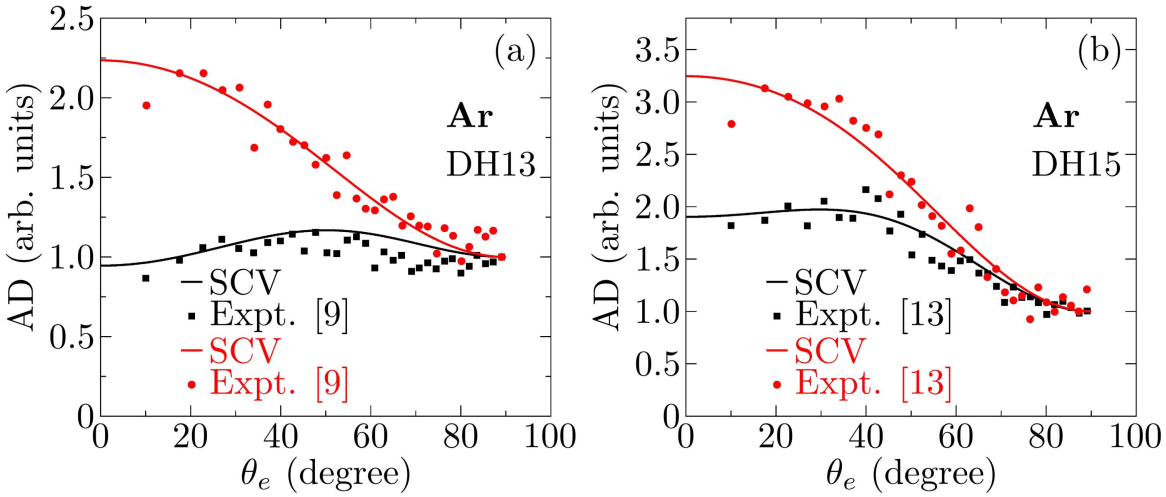

Figure 2. (a) Argon APT-NIR angular distributions for the DH13 line with $\phi_L = 0.144\pi$ (black) and $\phi_L = 0.644\pi$ (red). (b) Same as (a) but for the DH15 line with $\phi_L = 0.188\pi$ (black) and $\phi_L = 0.688\pi$ (red). The asymptotic photoelectron energy is (a) $p_q^2/2 = 4.28$ eV and (b) $p_q^2/2 = 7.40$ eV.

one found in previous second-order perturbation studies [1, 9]. The faster decay observed in the SB's angular distribution as compared to the DH ones for angles θ_e near 90° may be explained as the combination of the monochromatic $\cos^2\theta_e$ decay modulated in the SBs by the destructive interference predicted by equation (16) for $\theta_e = 90°$. The slight discrepancies observed between our theoretical predictions and the experimental data for emission angles near 90° may be attributed to our model that forbids the exchange of NIR photons for emission in directions perpendicular to the NIR polarization. In contrast, TDSE results show that the ADs of the SBs do not cancel completely at 90° [14].

In figure 2, we show ADs for the DHs of Ar targets, obtained with our model and compared to the available experimental data [9, 13]. We consider an NIR of intensity $I_L = 1.3 \times 10^{12}$ W cm^{-2} for figure 2(a) and $I_L = 0.76 \times 10^{12}$ W cm^{-2} for figure 2(b). The ADs are normalized at an emission angle of 90° and the asymmetry factor β corresponding to each of the asymptotic photoelectron energies were interpolated from theoretical data [26].

As can be seen, our results for Ar are in better agreement with the experiments than the ones for He. The same situation was observed for the soft-photon approximation [9]. At variance with the results for He atoms, constructive interferences predicted by equation (17) for emission at $\theta_e = 90°$ may be observed in the DH lines of Ar as the emission in this direction is not forbidden by the dipole selection rules. The evolution of the ADs as a function of the delay for emission angles near $\theta_e = 0°$ may be interpreted analogously to the He case.

So far, we proved that our analytical model is reasonably accurate in describing the ADs in several situations. Now, we proceed a step further by considering a higher NIR intensity and photoelectron energies satisfying the necessary conditions for the existence of nodes in DH lines coming from two-center interferences ($R_L > \lambda_q/2$ or $\mathbf{p}_q \cdot \mathbf{R}_L > \pi$).

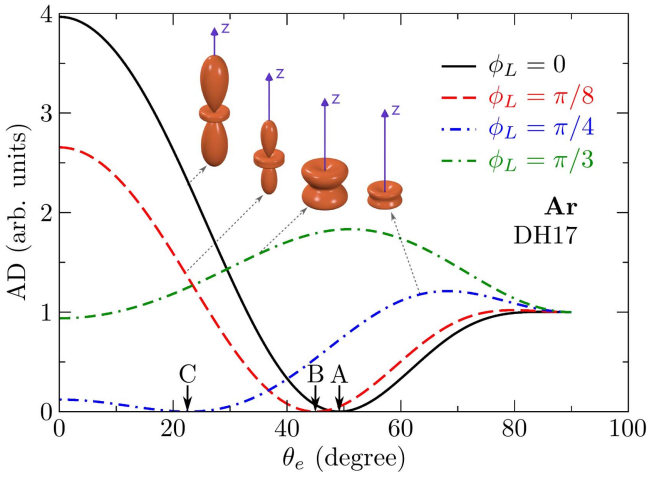

Figure 3. Argon APT-NIR angular distributions for the DH17 line for different delays ϕ_L. The considered NIR intensity is $I_L = 2.78 \times 10^{12}$ W cm^{-2}. The insets show the cylindrically symmetric three dimensional angular distributions. The asymptotic photoelectron energy is $p_q^2/2 = 10.38$ eV.

In figure 3, we show the angular distributions for the DH17 in Ar, for different delays ϕ_L and an NIR intensity of $I_L = 2.78 \times 10^{12}$ W cm^{-2}, that is about two or three times the values of the previous cases.

The angles labelled as A, B and C in figure 3 satisfy the relation $\cos(\mathbf{p}_q \cdot \mathbf{R}_L/2) = 0$ for different delays, showing that with a higher NIR intensity and/or photoelectron energy, it could be possible to observe nodes in the ADs. Moreover, these zeros have been also observed in *ab initio* calculations (figure (5) from [6]).

Also, it is clear that the angular position of these zeros moves towards $\theta_e = 0°$ as the delay ϕ_L increases from 0 to $\pi/3$, i.e., as the separation between the emitters is reduced. Finally, for $\phi_L = \pi/3$ no total destructive interferences are

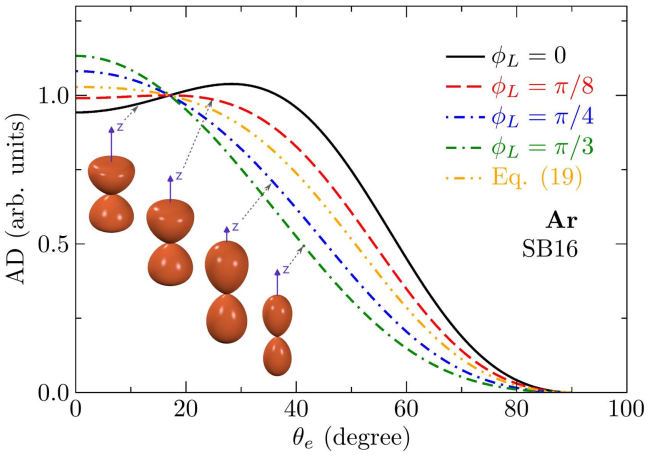

Figure 4. Argon APT-NIR angular distributions for the SB16 line for different delays ϕ_L. The remaining parameters are equal to those in figure 3. The insets show the cylindrically symmetric three dimensional angular distributions. he asymptotic photoelectron energy is $p_q^2/2 = 8.83$ eV.

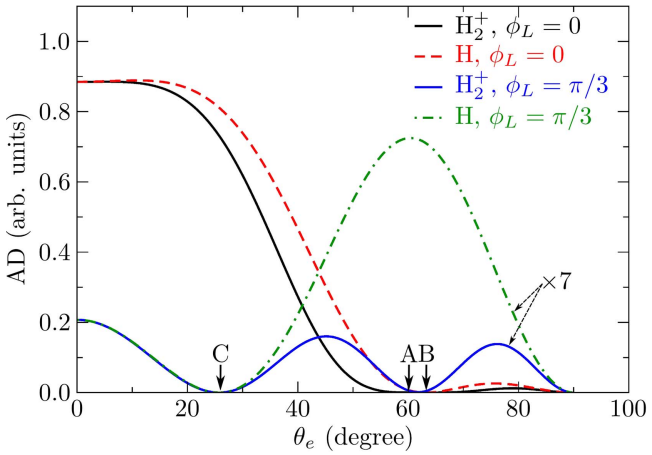

Figure 5. H_2^+ APT-NIR angular distributions for the asymptotic photoelectron momentum $p = 3.16$ and different delays ϕ_L. The considered NIR intensity is $I_L = 4.5 \times 10^{11}$ W cm^{-2}. The results for the hydrogenic atom are rescaled, for each delay, to the molecular ones at $\theta_e = 0°$.

observed because the separation R_L becomes smaller than half the photoelectron wavelength λ_q.

The results in figure 4 show the ADs for the SB16 in Ar normalized at the emission angle $\theta_e = 17°$, for different delays and the same NIR intensity as before. These results are different from those of He in figure 1(b) mainly because the ADs now show an evolution when different delays are considered. This evolution is related to the existence of effectively open channels involving a net exchange of more than one NIR photon. In contrast with our predictions, the results obtained with equation (19) in figure 4 are independent of the delay after normalization and thus unable to represent the trend observed for the different delays.

In addition, this also means that the SB modulation as a function of the delay no longer oscillates at twice the NIR frequency as expected from the low NIR intensity limit. In turn, this is in agreement with *ab initio* results where a distortion of the SB signal was found increasing the NIR intensity [27]. The advantage of our model is that it provides analytical expressions accounting for these modifications in the SB or DH lines.

Moreover, assuming that $p_q \sim p_{q+1}$, it is clear from equations (16) and (17) that the arithmetical sum of the differential cross sections of a dressed harmonic line and one of its neighbour lines (a sideband), should be proportional to the monochromatic photoionization differential cross section. In turn, this means that the increase (decrease) in DH lines comes from a decrease (increase) in the neighbour SB line signal, whether it is considered as a function of the delay or the NIR intensity.

It is worth mentioning that a further increase in the photoelectron energy or the NIR intensity may lead to angular distributions of SB lines with nodes at emission angles prescribed by the equation (16). The necessary conditions that must be fulfilled to obtain these nodes is $\mathbf{p}_q \cdot \mathbf{R}_L > 2\pi$, thus requiring twice the photoelectron momentum (or alternatively, twice the electric field amplitude) as compared with the dressed harmonic line case.

If an atomic target behaves as a diatomic molecule when ionized by a comb of odd harmonics in the presence of an assistant laser, then a natural question arises: how do these angular distributions change when molecular targets are considered? To address this question, we briefly compare the results for the simplest diatomic molecule (H_2^+) with those obtained for a fictitious hydrogen atom having the same ionization potential as the molecule.

In figure 5, we compare the atomic and molecular results for a dressed harmonic with $p_q = 3.16$ and different delays. The chosen NIR intensity is $I_L = 4.5 \times 10^{11}$ W cm^{-2}. The details about the computation of monochromatic transition amplitudes for the H_2^+ target can be found in [12].

As can be seen, the existence of another interference mechanism in the molecular case may have a profound impact in the angular distributions, according to the chosen delay. The angle labelled A in figure 5 corresponds to the totally destructive interference due to the coherent emission from both molecular centers. This interference mechanism is described approximately by the expression $\cos^2(\mathbf{p} \cdot \mathbf{R})$ [21, 22], where $\mathbf{R}$ is the internuclear separation of the molecule ($R = 2$ for H_2^+) and from which the angle A is obtained.

For $\phi_L = 0$, the angular distributions for atomic and molecular targets are similar. The angle B, for which $\cos(\mathbf{p} \cdot \mathbf{R}_L)$ in equation (17) is zero, lies close to the angle A and therefore the qualitative behaviour of the angular distributions does not change significantly.

The results for $\phi_L = \pi/3$ are more interesting. Firstly, as the wavelength of the photoelectron is similar to the internuclear separation R, the coherent emission from both molecular centers in the H_2^+ case presents a constructive interference for emission directions with $\theta_e \sim 0$. As can be seen in figure 5 this implies a nearly atomic behaviour for the angles $\theta_e <$ C. Moreover, this angle C defines the emission

direction for which total destructive interference among the channels opened by the NIR is expected, according to equation (17). Finally, as the emission angle increases up to 90°, major differences between the results of atomic and molecular targets are found. The molecule still presents a destructive interference for the angle A whereas the atomic target has the most probable emission direction at those angles, leading to strongly different angular distributions.

Thus, the inclusion of an additional interference mechanism present in molecular targets offers better opportunities for the control of electron dynamics, as the angular distributions in the molecular case can be steered to behave almost like an atom ($\phi_L = 0$) or to a mixed atomic and molecular behaviour ($\phi_L = \pi/3$) just by selecting different delays.

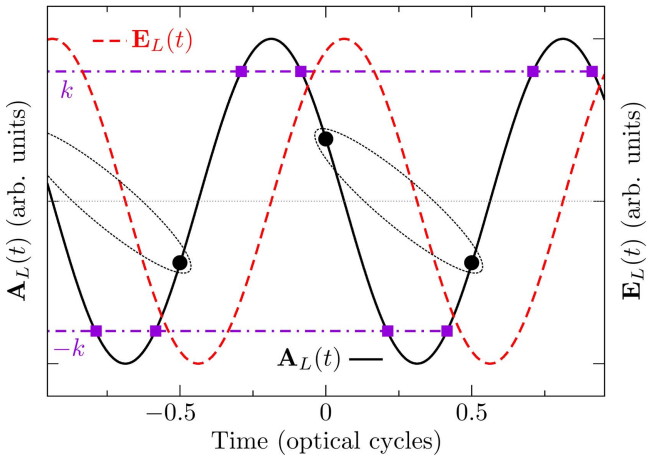

Figure 6. Comparison between the instantaneous vector potential value seen by the interfering wavepackets in the usual time-double slit and the laser-assisted ionization. In the former, interference is only possible for wavepackets launched to the continuum in times (purple squares) where the vector potential intersects the horizontal dash-dotted line corresponding to the asymptotic photoelectron momentum in the same semiplane. For the latter, the vector potential seen by consecutive wavepackets (black bullets surrounded by dotted ellipses) lies in opposite semiplanes.

4. Discussion

In order to get a physical insight about the meaning of the vector $\mathbf{R}_L$ defined previously we unitarily transform the wavefunctions of the initial and final channels of the reaction as well as the interaction Hamiltonian operator $\mathcal{H}_{\rm int} = \mathbf{A}(t) \cdot \hat{\mathbf{p}}$ in equation (1). This unitary transformation is defined by means of the operator $\mathcal{T} = \mathcal{T}_1\mathcal{T}_2$, where,

$$\mathcal{T}_1 = \exp\left[\frac{\mathrm{i}}{2}\int^t \mathbf{A}_L^2(t')\mathrm{d}t'\right], \tag{20}$$

and

$$\mathcal{T}_2 = \exp\left[\mathrm{i}\hat{\mathbf{p}} \cdot \boldsymbol{\alpha}(t)\right], \tag{21}$$

where we have defined the vector quantity

$$\boldsymbol{\alpha}(t) = \int^t \mathbf{A}_L(t')\mathrm{d}t' = \frac{\mathbf{E}_1}{\omega_0^2}\cos(\omega_0 t - \phi_L). \tag{22}$$

The operator $\mathcal{T}_1$ represents a time dependent phase shift related to the ponderomotive energy $U_p = E_1^2/4\omega_0^2$ and $\mathcal{T}_2$ is a translation operator that defines an active transformation, equivalent to describe the original states from the Kramers–Henneberger (KH) reference frame [28], which, in turn, follows the classical quiver motion $\boldsymbol{\alpha}(t)$ of a free electron in the laser field $\mathbf{E}_L(t)$. We note that within the dipole approximation, the following commutation relations are satisfied $[\mathcal{T}_1, \mathcal{T}_2] = [\mathcal{T}, \mathcal{H}_{\rm int}] = 0$.

The transformed initial and final wavefunctions are given by $\tilde{\Psi}_{i,f}(\mathbf{r}, t) = \mathcal{T}\Psi_{i,f}(\mathbf{r}, t)$ with the explicit representations

$$\tilde{\Psi}_i(\mathbf{r}, t) = \psi_i(\mathbf{r} + \boldsymbol{\alpha}(t))\mathrm{e}^{\mathrm{i}(I_p+U_p)t}\mathrm{e}^{\mathrm{i}M\sin(2\phi_L - 2\omega_0 t)}, \tag{23}$$

and

$$\tilde{\Psi}_f(\mathbf{r}, t) = \psi_f(\mathbf{r} + \boldsymbol{\alpha}(t))\mathrm{e}^{-\mathrm{i}p^2 t/2}\mathrm{e}^{-\mathrm{i}\mathbf{p}\cdot\boldsymbol{\alpha}(t)}, \tag{24}$$

respectively. We would like to emphasize that oscillating expressions for initial dressed states were found previously within the impulse Coulomb–Volkov approximation in the length gauge [29, 30], but in our case the oscillatory character of the initial state corresponds merely to the description of an initial unperturbed state from the KH reference frame.

In the transformed reference frame, the transition matrix amplitude reads,

$$M_{\rm SCV}(\mathbf{p}) = -\mathrm{i}\int_{-\infty}^{\infty} \mathrm{d}t\ \langle\tilde{\Psi}_f(\mathbf{r}, t)|\mathcal{T}\mathcal{H}_{\rm int}\,\mathcal{T}^\dagger|\tilde{\Psi}_i(\mathbf{r}, t)\rangle, \tag{25}$$

and replacing the expressions for the initial and final wavefunctions given by equations (23) and (24), taking into account that the operator $\mathcal{T}$ commutes with the interaction Hamiltonian and considering that the ionization of the target occurs almost instantaneously at times $t = j\pi/\omega_0$ [15, 16], we get (see the appendix),

$$M_{\rm SCV}(\mathbf{p}_q) \propto M_{ph}(\mathbf{p}_q)\mathrm{e}^{\mathrm{i}M\sin(2\phi_L)}(\mathrm{e}^{\mathrm{i}\mathbf{p}\cdot\boldsymbol{\alpha}_0} \mp \mathrm{e}^{-\mathrm{i}\mathbf{p}\cdot\boldsymbol{\alpha}_0}), \tag{26}$$

where $\boldsymbol{\alpha}_0 = \boldsymbol{\alpha}(0)$ and the plus (minus) sign correspond to the DHs (SBs) lines. Except for a global phase factor, the expressions in equation (26) are identical to the transition matrix elements, within the two-effective center approximation [23] for the monochromatic photoionization of a homonuclear diatomic molecule initially in an ungerade (gerade) state with internuclear separation $\mathbf{R}_L = 2\boldsymbol{\alpha}_0$.

The sense in which these spatial two-center interferences may be interpreted is the following. Due to the oscillatory character of the initial and final states in the KH reference frame and as the ionization step of the reaction occurs at almost defined different times, the reaction evolves in the final channel as if the photoelectron wavepackets were emitted from different positions in space.

As the interfering wavepackets are launched to the continuum at different times, a comparison with the usual time-double slit [31, 32] in the strong field ionization of atoms by a few-cycle intense laser field is appropriate. In this scheme, the wavepackets that interfere are released to the continuum at times where the vector potential assumes its unique value, as

shown by the purple squares in figure 6, giving rise to intracycle and intercycle interferences [33].

On the contrary, in our case the interfering wavepackets are released at times where the instantaneous values of the vector potential are not necessarily equal as shown by the black bullets surrounded by the dotted ellipse in figure 6 corresponding to the values of the vector potential seen by successive wavepackets. Moreover, they lie in different semispaces, as opposed to the temporal double slit where they are, necessarily, in the same semispace to interfere. In our case, consecutive wavepackets finally interfere due to the multicolour character of the ionizing field.

In this sense, our results are closer to those of the wavepacket interferometry in the streaking regime as in [15, 16, 34] despite that the ionizing signal in this scheme does not fulfil the validity conditions of our model for every possible delay. Nevertheless, our results may be useful to interpret some of the interferograms in this regime.

5. Conclusion

We have extended the separable Coulomb–Volkov model to the case of an ionizing field with many frequencies. Using our extended model we find for the first time analytical expressions for the angular distributions in the laser-assisted ionization of atomic targets that resemble the monochromatic ionization of molecular targets. The results of our model were compared to recent experimental results showing an agreement comparable to other methods at hand including approximations and *ab initio*. The strength of our results resides in the fact that they express for DH and SB lines the interaction between the photoelectron and the assistant laser field to all orders providing analytical expressions that reproduce the expected behaviour in the low NIR intensity limit. Moreover, taking advantage of the non-perturbative character of our model, we calculate the angular distributions for the photoionization of atomic targets assisted by a stronger laser field. We find that zeros in dressed harmonic lines, previously reported in *ab initio* simulations, may be interpreted as a destructive interference of wavepackets emitted from different positions in space. Also, we show that an increase of the laser intensity and/or photoelectron energies leads to an evolution of the sideband lines for different delays even when they are normalized. This evolution, related to the breakup of the low NIR intensity behaviour for these lines, is connected with the population transfer between dressed harmonic lines and sideband lines, whether it is considered as a function of the delay or the NIR intensity. In addition, we briefly study the case of molecular targets, showing that the angular distributions obtained for these targets can be steered to behave fully or partially as an atom, just by selecting different delays. Finally, by a unitary transformation we show that the emergence of the spatial two-center interference, obtained within our model, may be explained in terms of oscillating initial and final states when the reaction is described in the Kramers–Henneberger reference frame.

Acknowledgments

Authors acknowledge financial support from the Agencia Nacional de Promoción Científica y Tecnológica (PICT No. 01912), the Consejo Nacional de Investigaciones Científicas y Técnicas de la República Argentina (PIP No. 11220090101026), and the Fundación Josefina Prats.

Appendix A. Obtaining equations (12) and (13)

Starting from equation (8) for the transition matrix amplitude in the laser-assisted photoionization process, we note that the Gaussian factor is the only one that prevents the factorization into independent series as $\omega_j = p^2/2 + I_p + (2M + 2m + n - j)\omega_0$. As we are interested in the angular distributions for dressed harmonic lines or sideband lines, where the energy relation $p_q^2/2 + I_p + 2M\omega_0 = q\omega_0$ is satisfied, the ω_j factor assumes its final form $\omega_j = (2m + n + q - j)\omega_0$.

Now, if $\tau_T \gg \sqrt{2}/\omega_0$, which is true for APTs with many pulses, then the Gaussian factor behaves as,

$$\mathrm{e}^{-\omega_j^2\tau_T^2/2} = \begin{cases} 1 & \text{if } j = 2m + n + q, \\ \mathcal{O}(\mathrm{e}^{-\alpha^2/2}) & \text{otherwise} \end{cases} \tag{A.1}$$

where $\alpha = \tau_T|2m + n + q - j|\omega_0 \gg 1$. Under these conditions, the terms with $j \neq 2m + n + q$ may be omitted, i.e., the Gaussian factor may be replaced by the Kronecker delta $\delta_{j,2m+n+q}$. Then, the triple sum in equation (8) turns into a double sum, where the mixed dependence of each term on the independent indices m and n is encoded into the phases ϕ_{2m+n+q} and the amplitudes A_{2m+n+q}.

A combination of harmonics, as the one in equation (2), produces a train of pulses with a sub-femtosecond duration only if harmonics are phase-locked. Therefore, we adopt the widespread theoretical approach of considering a combination of in-phase harmonics with equal amplitudes A_j [6, 27], which in turn allows the factorization of these index-dependent phases and amplitudes as a global factor. Then, the triple sum in equation (8) may be factorized as the product of two independent series,

$$M_{\mathrm{SCV}}(\mathbf{p}_q) = B_0 M_{ph}(\mathbf{p}_q) \sum_m (-1)^m J_m(M) \mathrm{e}^{-\mathrm{i}2m\phi_L} \times \sum_n i^n J_n(N) \mathrm{e}^{-\mathrm{i}n\phi_L}, \tag{A.2}$$

where $B_0 = -\mathrm{i}\sqrt{2\pi}\,\tau_L A_0$ and A_0 is the constant amplitude of each harmonic.

Now, these series can be evaluated analytically invoking the complex- and real-valued Jacobi–Anger expansions [35] but before we proceed any further it is necessary to separate the cases under study. As we show below, parity considerations among the integer numbers j, n and q play a crucial role. On the contrary, the index m is not relevant because it is multiplied by two in $j = 2m + n + q$.

Firstly, if the APT is an even-odd combination of harmonics, the index j runs on even and odd integer numbers. Moreover, as the parameter q can be also even or odd, the Kronecker delta does not impose restrictions over the set of

values assumed by n. In this case, the transition matrix element reads,

$$M_{\mathrm{SCV}}(\mathbf{p}_q) = B_0 M_{ph}(\mathbf{p}_q) \mathrm{e}^{\mathrm{i}M \sin(2\phi_L)}\, \mathrm{e}^{\mathrm{i}N \cos\phi_L}, \tag{A.3}$$

where we make use of the complex-valued Jacobi–Anger expansions to obtain the analytical sum of each series in equation (A.2).

Secondly, if the APT is a combination of odd harmonics, the index j only assumes odd integer values. As the parameter q, describing the photoline of interest, can be an even or odd integer number, parity considerations in the relation $j = 2m + n + q$ impose restrictions over the set of values that the index n may assume. Accordingly, we separate the results for q an even or odd integer number.

For q an even number (SBs), the index n can only assume odd integer values to satisfy the parity considerations, in agreement with the physical picture of SBs populated only by transitions involving a net exchange of an odd number of NIR photons. In this case, the transition matrix amplitude is given by

$$M_{\mathrm{SCV}}(\mathbf{p}_q) = \mathrm{i}B_0 M_{ph}(\mathbf{p}_q) \mathrm{e}^{\mathrm{i}M \sin(2\phi_L)} \sin(N \cos\phi_L), \tag{A.4}$$

where the complex- and real-valued Jacobi–Anger expansions are used to obtain the analytical sum of each series in equation (A.2).

On the other hand, for q an odd number (DHs), the index n can only assume even integer numbers to satisfy the parity considerations, in agreement with the physical picture of DHs populated only by transitions involving a net exchange of an even number of NIR photons. Accordingly, the transition matrix amplitude is given by,

$$M_{\mathrm{SCV}}(\mathbf{p}_q) = B_0 M_{ph}(\mathbf{p}_q) \mathrm{e}^{\mathrm{i}M \sin(2\phi_L)} \cos(N \cos\phi_L). \tag{A.5}$$

Appendix B. Obtaining equation (26)

Starting from equation (25), replacing the expressions for the initial and final wavefunctions given by equations (23) and (24) and taking into account that the operator $\mathcal{T}$ commutes with the interaction Hamiltonian, we get

$$M_{\mathrm{SCV}}(\mathbf{p}) = -\mathrm{i} \int_{-\infty}^{\infty} \mathrm{d}t\; M_{ph}(\mathbf{p}_q, t) \mathrm{e}^{\mathrm{i}\mathbf{p}\cdot\boldsymbol{\alpha}(t)} \times \mathrm{e}^{\mathrm{i}M \sin(2\phi_L - 2\omega_0 t)} \mathrm{e}^{\mathrm{i}(p^2/2 + I_p + U_p)t}, \tag{B.1}$$

where the 'time-dependent' monochromatic transition matrix element is given by

$$M_{ph}(\mathbf{p}_q, t) = \langle \psi_f(\mathbf{r} + \boldsymbol{\alpha}(t)) | \mathbf{A}(t) \cdot \hat{\mathbf{p}} | \psi_i(\mathbf{r} + \boldsymbol{\alpha}(t)) \rangle. \tag{B.2}$$

The key to factorize this transition matrix element is to note that it depends on time only through the vector potential $\mathbf{A}(t)$. In fact, in the velocity gauge, the spatial integral involved

$$M_{ph}(\mathbf{p}_q, t) \propto -\mathrm{i} \int \mathrm{d}^3 r\; \psi_f^*(\tilde{\mathbf{r}})\, \boldsymbol{\Pi} \cdot \nabla_r \psi_i(\tilde{\mathbf{r}}) = M_{ph}(\mathbf{p}_q), \tag{B.3}$$

is time independent, as can be seen making the transformation $\mathbf{r} \to \tilde{\mathbf{r}}$, with $\tilde{\mathbf{r}} = \mathbf{r} + \boldsymbol{\alpha}(t)$. Such a transformation leaves the last integral unaffected, irrespective of the $\boldsymbol{\alpha}(t)$ value.

Finally, as the ionization of the target by the APT can be considered to occur almost instantaneously at times fixed by the time dependent part of the vector potential $\mathbf{A}(t)$, and taking into account that the APT contains two opposite pulses per NIR cycle [6, 15, 16], the time integration in equation (B.1) may be approximated by the sum over two consecutive times $t = j\pi/\omega_0$, and we get

$$M_{\mathrm{SCV}}(\mathbf{p}_q) \propto M_{ph}(\mathbf{p}_q) \mathrm{e}^{\mathrm{i}M \sin(2\phi_L)} (\mathrm{e}^{\mathrm{i}\mathbf{p}\cdot\boldsymbol{\alpha}_0} \mp \mathrm{e}^{-\mathrm{i}\mathbf{p}\cdot\boldsymbol{\alpha}_0}), \tag{B.4}$$

where we defined $\boldsymbol{\alpha}_0 = \boldsymbol{\alpha}(0)$ and use the fact that $\boldsymbol{\alpha}(t + \pi/\omega_0) = -\boldsymbol{\alpha}(t)$. The minus (plus) sign correspond to the SBs (DHs) lines.

References

[1] Paul P M, Toma E S, Breger P, Mullot G, Augé F, Balcou P, Muller H G and Agostini P 2001 *Science* **292** 1689–92
[2] Hentschel M, Kienberger R, Spielmann C, Reider G A, Milosevic N, Brabec T, Corkum P, Heinzmann U, Drescher M and Krausz F 2001 *Nature* **414** 509–13
[3] Kelkensberg F *et al* 2011 *Phys. Rev. Lett.* **107** 043002
[4] Laurent G, Cao W, Li H, Wang Z, Ben-Itzhak I and Cocke C L 2012 *Phys. Rev. Lett.* **109** 083001
[5] Dahlström J M, L'Huillier A and Maquet A 2012 *J. Phys. B: At. Mol. Opt. Phys.* **45** 183001
[6] Galán A J, Argenti L and Martín F 2013 *New J. Phys.* **15** 113009
[7] Maquet A and Taïeb R 2007 *J. Mod. Opt.* **54** 1847–57
[8] Meyer M *et al* 2008 *Phys. Rev. Lett.* **101** 193002
[9] Picard Y J *et al* 2014 *Phys. Rev.* A **89** 031401
[10] Yudin G L, Patchkovskii S, Corkum P B and Bandrauk A D 2007 *J. Phys. B: At. Mol. Opt. Phys.* **40** F93
[11] Yudin G L, Chelkowski S and Bandrauk A D 2006 *J. Phys. B: At. Mol. Opt. Phys.* **39** L17
[12] Boll D I R and Fojón O A 2014 *Phys. Rev.* A **90** 053414
[13] Weber S J *et al* 2015 *Rev. Sci. Instrum.* **86** 033108
[14] Guyétand O *et al* 2005 *J. Phys. B: At. Mol. Opt. Phys.* **38** L357
[15] Remetter T *et al* 2006 *Nat Phys* **2** 323–6
[16] Varjú K *et al* 2006 *J. Phys. B: At. Mol. Opt. Phys.* **39** 3983
[17] Guyétand O *et al* 2008 *J. Phys. B: At. Mol. Opt. Phys.* **41** 051002
[18] Kazansky A K and Kabachnik N M 2007 *J. Phys. B: At. Mol. Opt. Phys.* **40** 2163
[19] Cionga A, Florescu V, Maquet A and Taïeb R 1993 *Phys. Rev.* A **47** 1830–40
[20] Zhang C H and Thumm U 2010 *Phys. Rev.* A **82** 043405
[21] Cohen H D and Fano U 1966 *Phys. Rev.* **150** 30–3
[22] Walter M and Briggs J 1999 *J. Phys. B: At. Mol. Opt. Phys.* **32** 2487
[23] Weck P, Fojón O A, Hanssen J, Joulakian B and Rivarola R D 2001 *Phys. Rev.* A **63** 042709
[24] Ciappina M F, Fojón O A and Rivarola R D 2014 *J. Phys. B: At. Mol. Opt. Phys.* **47** 042001
[25] Cooper J and Zare R N 1968 *J. Chem. Phys.* **48** 942–3
[26] Huang K N, Johnson W and Cheng K 1981 *At. Data Nucl. Data Tables* **26** 33–45
[27] Mauritsson J, Gaarde M B and Schafer K J 2005 *Phys. Rev.* A **72** 013401
[28] Henneberger W C 1968 *Phys. Rev. Lett.* **21** 838–41
[29] Macri P A, Miraglia J E and Gravielle M S 2003 *J. Opt. Soc. Am.* B **20** 1801–6
[30] Gravielle M S, Arbó D G, Miraglia J E and Ciappina M F 2012 *J. Phys. B: At. Mol. Opt. Phys.* **45** 015601

[31] Lindner F, Schätzel M G, Walther H, Baltuška A, Goulielmakis E, Krausz F, Milošević D B, Bauer D, Becker W and Paulus G G 2005 *Phys. Rev. Lett.* **95** 040401
[32] Gopal R *et al* 2009 *Phys. Rev. Lett.* **103** 053001
[33] Arbó D G, Ishikawa K L, Schiessl K, Persson E and Burgdörfer J 2010 *Phys. Rev.* A **81** 021403
[34] Mauritsson J, Johnsson P, Mansten E, Swoboda M, Ruchon T, L'Huillier A and Schafer K J 2008 *Phys. Rev. Lett.* **100** 073003
[35] Gradshteyn I S and Ryzhik I M 2007 *Table of Integrals, Series, and Products* 7th edn (Amsterdam: Elsevier/Academic Press)